ChemComm

Accepted Manuscript

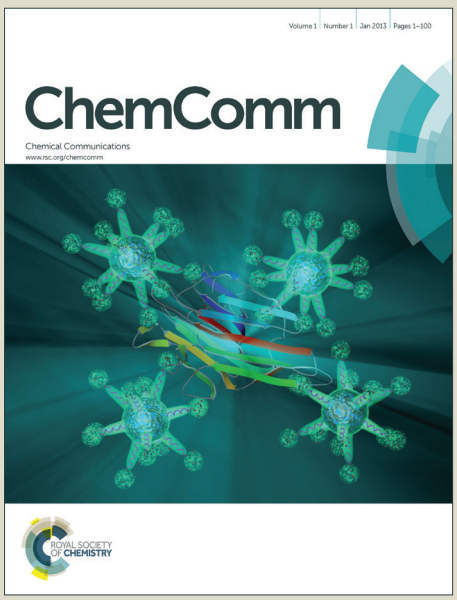

ROYAL SOCIETY OF CHEMISTRY

www.rsc.org/chemcomm

Chemical Communications RSCPublishing

Feature ARTICLE

Studying the dynamic behaviour of porphyrins as prototype functional molecules by scanning tunnelling microscopy close to room temperature

Cite this: DOI: 10.1039/x0xx00000x

Received 00th January 2012,
Accepted 00th January 2012

DOI: 10.1039/x0xx00000x

www.rsc.org/

H. Marbach* and H.-P.Steinrück

Scanning tunnelling microscopy (STM) enables to directly observe the dynamic behaviour of organic molecules on surfaces. While imaging atoms and molecules in STM is certainly fascinating by itself, corresponding temperature-dependent measurements allow for the quantitative determination of the energetics and kinetics of the underlying molecular surface processes. Herein, we review recent advances in the STM investigation of the dynamic behaviour of adsorbed porphyrins at and close to room temperature. Three different case studies are discussed, providing insight in the dynamics of diffusion, rotation, reaction, and molecular switching at surfaces, based on isothermal STM measurements. The reviewed examples demonstrate that variable temperature STM can be a suitable tool to directly monitor the dynamic behaviour of individual adsorbed molecules, at and close to room temperature. Free-base porphyrins on Cu(111) proved to be particularly suitable for these studies due to the strong bonding interaction between the iminic nitrogen atoms in the porphyrin macrocycle with the Cu substrate atoms. As a consequence, the corresponding activation energies for surface diffusion, self-metalation reaction and conformational switching are of a magnitude that allows for monitoring the processes around room temperature, in contrast to most previous studies, which were performed at cryogenic temperatures. The kinetic analysis for the surface diffusion and self-metalation was performed using an Arrhenius approach, yielding the corresponding activation energies and preexponential factors. In contrast, the conformational switching process was analysed in the framework of transition state theory, based on the Eyring equation. This approach provides a more detailed insight into interpretable thermodynamic potentials, i.e., the enthalpic and entropic contributions to the activation barrier. The analysis shows that at room temperature the adsorption and switching behaviour of the investigated free base porphyrin on Cu(111) is dominated by entropic effects. Since the entropic energy contribution vanishes at low temperatures, the importance of experiments conducted at temperatures close to room temperature is emphasized.

1 Introduction

With the invention of the scanning tunnelling microscope (STM) in the early 80's of the last century[1] the direct real space observation of atoms and molecules on extended surfaces of solids became possible. Based on its unparalleled capabilities, STM was quickly established as a powerful tool in fundamental sciences and is nowadays a standard instrument in laboratories all over the world. Among manifold STM-based research activities, the investigation of large organic molecules on surfaces has become a vivid field in science with the vista to engineer functional devices[2, 3]. Specific interactions between absorbed molecules and/or with the underlying substrate often trigger peculiar adsorption behaviours like the self-assembly into long range ordered arrays or the occurrence of individual isolated molecules. Due to their versatility, the molecules from the "porphyrin family" are considered as ideal building blocks for the generation of functional molecular devices: they combine a rigid planar framework as structure forming element with an intrinsic functionality, which is mainly determined by the coordinated metal center[4]. The importance of porphyrins is highlighted by their omnipresence as main functional building blocks in nature[5] — examples are iron porphyrin in heme[6] or magnesium porphyrin in chlorophyll[7] — but also due to their application in sensor[8, 9] and solar cell technology[10-15]. The enormous potential of porphyrins for the fabrication of tailor-made functional molecular architectures on well-defined substrates has stimulated significant activities in fundamental research[4, 16-32].

In this contribution, we review recent advances in the understanding of the dynamic behaviour of porphyrins, as representatives of organic molecules, adsorbed on the Cu(111) single crystal surface in ultra-high vacuum (UHV). Based on temperature-dependent measurements of individual molecules, the kinetics and energetics of diffusion[33, 34] and rotation[34], of the so-called self-metalation reaction[35, 36] and finally of conformational switching of particular free base porphyrins[37] can be determined. Even though these processes appear to be very different at first glance, they can all be regarded as activated processes, as schematically sketched in Figure 1. The standard method to extract quantitative information from temperature-dependent data of such surface processes is the Arrhenius analysis. Svante Arrhenius developed his famous equation on a purely empirical basis and published it at the end of the 19th century[38].

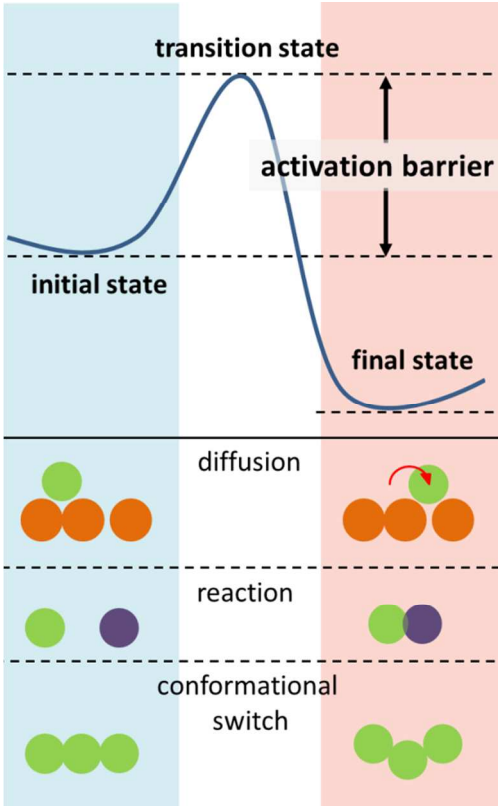

Fig. 1 Generalized energy scheme for an activated process (top), and three corresponding examples (diffusion, reaction and conformational switching).

The general form of the Arrhenius equation is:

$$r(\mathrm{T}) = A \cdot e^{-\frac{E}{k_B T}}$$

with *r(T)* being the temperature-dependent rate, *A* the so-called preexponential factor and *E* the activation barrier or energy (see Fig. 1) of the investigated process (k_B: Boltzmann constant, *T*: Temperature). While the activation energy *E* is intuitively accessible and the exponential dependency can be comprehended by regarding the Maxwell-Boltzmann statistics, the interpretation of the preexponential factor *A* is somewhat more difficult. For first order processes, to which all processes discussed in this feature article belong to, the dimension of *A* is s^{-1}. Therefore, *A* is also often referred to as frequency factor, somewhat naively implying that the involved molecule vibrates with a frequency given by *A* in the relevant potential; in some cases, this interpretation can be correct, but in others it is certainly misleading.

An alternative and fully comprehensible interpretation of the preexponential factor was deduced in the frame of the transition state theory (TST) by Eyring and co-workers[39]. In TST, the activation barrier (see Figure 1) is defined as the difference in Gibbs energy, $\Delta G^{\#}$, of the initial and the transition state. With the introduction of the thermodynamic potential $\Delta G^{\#}$ and by considering the Gibbs-Helmholtz equation, $\Delta G^{\#} = \Delta H^{\#} - T\Delta S^{\#}$, the temperature-dependent rate follows as

$$r(T) = \left(\frac{k_B T}{h}\right) \cdot e^{-\frac{\Delta G^{\#}}{k_B T}} = \left(\frac{k_B T}{h}\right) \cdot e^{\frac{\Delta S^{\#}}{k_B}} e^{-\frac{\Delta H^{\#}}{k_B T}}$$

the so-called Eyring Equation. A more detailed discussion of this equation will be given in Section 4 below. Nevertheless, one can already state here that the analysis of the temperature-dependence of the reaction rate gives direct access to the contributions of the thermodynamic potentials $\Delta H^{\#}$ and $T\Delta S^{\#}$ to the Gibbs energy, $\Delta G^{\#}$. Since the entropic contribution, $T\Delta S^{\#}$, scales with *T*, it is immediately clear that it vanishes at low temperatures. Consequently, in low temperature (LT) STM measurements entropic effects practically do not play a role. Therefore, such effects can only be studied by performing experiments at higher temperatures. In turn, if one performs experiments at higher temperatures, entropic contributions should be considered in order to obtain a detailed understanding of the energetics of a process. Herein, we review results obtained at and close to room temperature (RT), not only because such measurements are closer to realistic conditions for applications, but also since they allow for investigating the role of entropic effects. The comparison of the Arrhenius equation and the Eyring equation reveals that the preexponential factor *A* linearly depends on T and contains a term that depends on the entropy difference between initial and transition state, $\Delta S^{\#}$:

$$A = \left(\frac{k_B T}{h}\right) \cdot e^{\frac{\Delta S^{\#}}{k_B}}$$

Note that for $\Delta S^{\#} = 0$ and a temperature of 480 K, *A* equals 10^{13} s^{-1}, which is the value typically used as first order approximation of the preexponential factor, if no other information is available.

In the first two examples discussed below, i.e., for diffusion and rotation, and for the self-metalation reaction on surfaces, the kinetic analysis is performed using the Arrhenius equation, as typically done in surface science. For the third example, which addresses conformational switching of molecules on surfaces, the analysis is based on the Eyring equation, because a

detailed insight in the thermodynamic potential was required in order to understand to observed complex behaviour.

2 Diffusion and Rotation of 2HTPP

The diffusion dynamics of adsorbates on surfaces are of fundamental interest in surface science and constitute the basis for the self-assembly of functional molecular architectures in a bottom-up approach[16, 40]. STM has proven to be a suitable tool for the investigation of surface migration and the determination of the corresponding kinetic parameters. While initially mainly the surface diffusion of atoms or small molecules on metal surfaces [41-45] was addressed, in the last decade also large organic molecules were investigated[46]; these studies include decacyclen and hexa-tert-butyl-decacyclene on Cu(111)[47], dithioanthracene on Cu(111)[48], 4-trans-2-(pyrid-4-yl-vinyl) benzoic acid on Pd(110)[49], C_{60} on Pd(110)[50], tris-(2-phenylpyridine)iridium(III) on Cu (111)[51], and 2H-tetrapyridyl-porphyrin (2HTPyP) on Cu(111)[33]. The latter study by Eichberger et al. represents the first example for the direct observation of the unidirectional motion of porphyrins at 300 K and above, i.e., at comparably high temperatures, by STM. The fact that this was possible, is especially remarkable, since porphyrins usually rapidly diffuse on the time scale of STM at RT and thus cannot be imaged as individual molecules[52]. However, for 2HTPyP and also for the very similar 2H tetraphenylporphyrin (2HTPP) (which will be discussed in detail below) the molecules can indeed be imaged as isolated individual entities at RT on Cu(111) [33, 34, 36, 37, 53-58]. The reason for the very peculiar adsorption behaviour of these free base porphyrins on Cu(111) is a strong site-specific attractive interaction between the iminic nitrogen atoms of the porphyrin macrocycle and the Cu substrate atoms; this specific interaction was already suspected in[33, 55] and later on verified by XPS[59]. In the following, the specific role and interplay of adsorbate-substrate and adsorbate-adsorbate interactions of different tetra-phenylporphyrins (2HTPP and CoTPP) on Ag(111) and Cu(111) will be discussed. The STM images in Figure 2a and 2b illustrate the island formation, i.e., the self-assembly behaviour of tetraphenylporphyrins (TPP) on Ag(111) at RT. For TPPs without a central metal atom, i.e., 2HTPP, and also for metalloporphyrins with various central metal atoms (e.g., Co, Fe, Zn, Ni), always the formation of square arrays with a lattice constant of 1.40 ± 0.05 nm is observed[52]. In addition, different TPP species (e.g., 2HTPP and CoTPP) statistically intermix in the square arrangement without any detectable spatial correlation. The driving force for the formation of this supramolecular order is a mutual stabilization mediated by so-called T-type interaction between the phenyl groups of neighbouring molecules[52, 60]. The same behaviour, namely the island formation with a square lattice from a certain coverage on, is also observed for CoTPP and CuTPP on Cu(111).

A completely different behaviour is observed for 2HTPP on Cu(111), as is evident from the STM image depicted in Fig 2 c, where no island formation is found at low and medium coverages. In contrast, individual molecules can be identified; this behaviour is attributed to the above mentioned site-specific coordinative bond between the iminic nitrogen atoms of the porphyrin macrocycle and the Cu atoms. As a consequence of this interaction, the molecule is literally pulled toward the surface, as indicated in Figure 2e, which results in a nearly flat

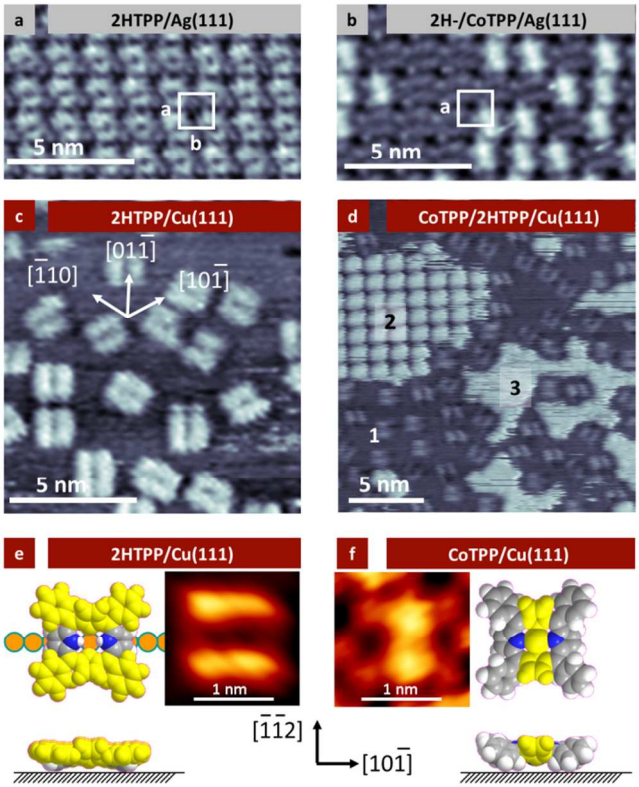

Figure 2. Constant current RT STM images: (a) A monolayer of 2HTPP on Ag(111) (U=+0.45 V, I=25 pA); (b) Intermixed 2HTPP/CoTPP monolayer with a ratio of 2:1 on Ag(111); the bright longish protrusions correspond to CoTPPs; (U=-1.35 V, I=35 pA); (c) 2HTPP on Cu(111) (U=-0.77 V, I=26 pA),); (d) Mixed 2HTPP/CoTPP coverage on Cu(111) (U=-1.94 V, I=27 pA). Molecules indicated with 1 are individual 2HTPPs, the square array marked with 2 is a self-assembled square array from CoTPP. The bright regions labelled with 3 are highly mobile CoTPP molecules. (e) STM image of an individual 2HTPP with the corresponding scaled space-filling model (U= -1.49 V, I=30 pA). A closed packed Cu atomic row is indicated, highlighting the coordinative bond between the iminic nitrogen atoms of 2HTPP and the copper substrate atoms (f) STM image of a single CoTPP with the corresponding scaled space-filling model (U= -1.48 V, I=27 pA). All bias voltages given in the work at hand refer to the sample. The parts marked yellow in the models are the topographically highest parts of the molecules. (Adapted with permission from Buchner et al.[55] Copyright 2011 Wiley)

conformation with the phenyl rings almost parallel to the surface; this geometry leads to the characteristic appearance of the molecule with two longish parallel protrusions, which is shown in Figure 2e. The orientation of the phenyl rings nearly parallel to the surface effectively inhibits the mentioned attractive T-type interactions between neighbouring molecules, which explains why 2HTPP does not form two-dimensional islands on Cu(111). We also want to mention a somewhat different interpretation, given by Rojas et al., who propose a considerable charge transfer from the Cu(111) substrate to the 2HTPP which results in repulsive dipole-dipole interaction between the free base porphyrins[54, 61]. However, Buchner et al. found no indications for such a massive charge transfer; such indications would be an asymmetric appearance of 2HTPP upon switching the polarity of the bias voltage or reduced residence times and changed velocities for 2HTPPs at small intermolecular distances[55]. Still, one cannot rule out that both proposed effects might contribute to the observed behaviour.

To illustrate the different adsorption behaviour of 2HTPP and metalloporphyrins at submonolayer coverages on Cu(111), a mixture of 2HTPP and CoTPP was deposited on Cu(111). The corresponding STM image in Figure 2d shows a phase separation of the two species. 2HTPPs appear as isolated molecules, as in pure 2HTPP layers. On the other hand, CoTPPs form well-ordered islands with a square unit cell. The appearance of CoTPP in the STM image with submolecular resolution in Figure 2f is dominated by the two pyrrole groups, which are bent away from the surface. This specific appearance of individual TPPs in STM is due to a saddle-shape distortion of the molecule and is well established in the literature[52, 60].

In Figure 2d, the regions with isolated 2HTPP molecules are labelled with "1" and regions, where CoTPP forms islands with "2". In corresponding RT STM movies one occasionally observes CoTPP molecules which attach at and detach from the rim of the island, indicating a high mobility of isolated CoTPPs. Indeed, the bright, unstructured regions labelled with "3" in Figure 2d are assigned to CoTPP molecules diffusing fast under the STM tip. This illustrates that CoTPPs are also present in a 2D gas phase on the surface. Such molecules are not directly visible as individual molecules in the STM under the actual imaging conditions due to their high mobility[62-64]. The observed effective phase separation of 2HTPP and CoTPP on Cu(111) results from the fact that the adsorption of the free base 2HTPP is dominated by molecule-substrate interactions, while the supramolecular arrangement of CoTPP is caused by attractive molecule-molecule interactions.

Figure 3 provides a more detailed insight into the specific adsorption behaviour of 2HTPP on Cu(111). The figure shows that only three different azimuthal orientations are found, which are rotated with respect to each other by 120°. This means that the molecules are aligned along one of the three symmetry-equivalent densely packed substrate <110> directions, which are indicated as white arrows in the right lower corner of Figure 3a. The observation of isolated 2HTPPs at RT indicates a low mobility compared to, e.g., CoTPP on Cu(111), which cannot be imaged as individual molecules at this temperature (see above).

Next, the dynamic behaviour of 2HTPP on Cu(111) is reviewed in detail. In the two subsequently recorded STM images of the same surface region in Figure 3b and 3c (sample temperature: 301 K; time interval: ~ 265 s) three molecules with identical orientation can be recognized. When comparing the two images, it becomes evident that the positions of two of the molecules changed in a very specific way (note that the positions of the molecules in Figure 3b are indicated by white crosses in Figure 3c):

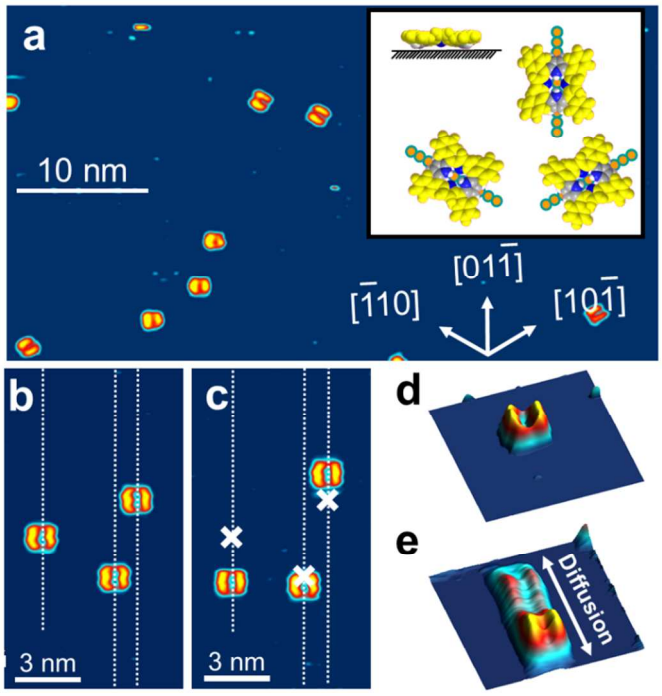

Figure 3 (a) Constant current STM image of 2HTPP on Cu(111) at low coverage, obtained at 301 K. The space-filling model in the insert exhibits the proposed intramolecular saddle-shape conformation and depicts the orientation relative to the Cu surface atoms along the surface <110> directions. (b) and (c) Subsequently recorded images of the same scan area: the position of the molecules in (b) are highlighted in (c) with crosses; the dashed white lines indicate the directions of the one-dimensional diffusion. (d) Pseudo three-dimensional STM image of a single 2HTPP and (e) the average STM frame of the corresponding STM time lapse movie (37 images with 20 seconds acquisition time each), with the elongated shape emphasizing the unidirectional diffusion. [(a)-(e) U = -1.49 V, I = 30 pA]. (Adapted with permission from Buchner et al.[34]. Copyright 2011 American Chemical Society)

For both, one-dimensional displacements along the high-symmetry substrate direction occurred, along which the molecules were aligned (indicated with dash-dotted lines). The one-dimensional motion can be even better illustrated by inspecting the average frame of a corresponding STM movie (37 images) acquired at 301 K in Figure 3e. The average frame appears as an elongated version of the two parallel protrusions of the single frame in Figure 3d. This behaviour indicated an

unidirectional motion of 2HTPP on Cu(111). Considering the moderate displacement per time (e.g., far below 5 nm per 265 s in Fig 2 c), the tracing of individual 2HTPP becomes possible by STM, even at the comparable high temperature of 301 K. This enables temperature-dependent measurements of the displacement of individual porphyrins around RT. When performing such measurements, one needs to ensure an undistorted thermally induced motion of the molecules, i.e., the influence of the STM measurements must be ruled out or at least minimized. In this context, it is beneficial that the

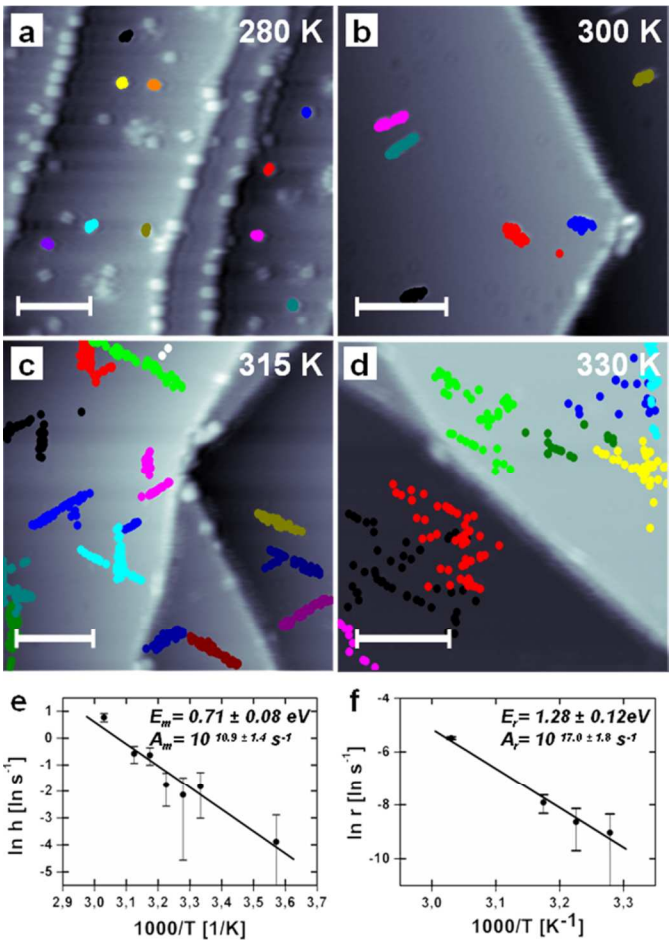

Figure 4 (a)-(d) Average frames of STM movies of 2HTPP on Cu(111) between 280 and 330 K (scale bar = 10 nm). The positions of the molecules were color-coded in each single STM image and then superimposed over the corresponding STM average frames [(a) U = -1.51 V, I = 29 pA; (b)–(d) U = -1.49 V, I = 30 pA]. (e) Arrhenius plot of the hopping rates vs. temperature. (f) Arrhenius plot of the rotational change of the diffusion direction. (Adapted with permission from Buchner et al.[34]. Copyright 2011 American Chemical Society)

2HTPP/Cu(111) system can be imaged with a high tunnelling resistance (U ~ 1.5V, I ~ 30 pA, R ~ 50 GΩ), which allow to avoid tip induced effects. Note that diffusion measurements by STM found in literature are typically carried out at tunnelling resistances in the range of 1 - 10 GΩ[33, 47-49, 65]. Since the tunnel resistance in the experiments by Buchner et al. [34] is even higher, i.e., the tip substrate interaction is lower, a significant influence of the STM measurement on the thermally induced diffusion can be practically ruled out. In addition, no influence upon changing image size, scanning speed and the fast scan direction (vertical/horizontal) was reported. To avoid the influence of intermolecular interactions (collisions), the 2HTPP coverage was kept sufficiently low in the corresponding experiments.

Following this approach, STM movies at different temperatures between 280 and 345 K were acquired (see SI of [34]). These movies comprise roughly 50 images with an acquisition time of 20 – 40 s/image, allowing for the analysis of roughly 2500 diffusion events. Figure 4 a-d present the average frames (superposition of the image series) at four temperatures. To illustrate the movement of the 2HTPPs the position of each molecule was marked in the images with a specific colour. The resulting traces of the individual molecules illustrate the temperature-dependent diffusion behaviour. Briefly, the behaviour at the different temperatures in Figure 4 can be described as follows: 280 K (a): 2HTPP molecules are confined to their adsorption sites, i.e., the circular or only slightly elongated dots indicate that no detectable movement occurs in the timeframe of the experiment; 301 K (b): unidirectional trajectories along one of the three high-symmetry directions of the surface are observed; 315 K (c): unidirectional trajectories with increased length are seen, with occasional changes of the direction of the trajectories by ± 120°, i.e., to one of the other high-symmetry substrate axes; 330 K (d): a further increase of the diffusion length and more frequent directional changes are found. For 345 K (not shown), the molecular diffusion is so fast that changes in the images already occurred on a time scale shorter than required to obtain one image, and the displacements were partly larger than the scan area. These data can therefore not be considered in the kinetic analysis. The quantitative analysis was performed using the procedure described by Eichberger et al. [33]: In a first step, the molecular displacements between consecutive images were evaluated for each temperature. From these data, the mean square displacement $\langle(\Delta x)^2\rangle$ and correspondingly the hopping rate[66] $h(T) = \langle(\Delta x)^2\rangle/(\langle\lambda\rangle^2 t)$ for each of the investigated temperatures were determined (λ is the jump length, i.e., the lattice constant of 2.55 Å along the <110> directions and t is the corresponding time interval).

To analyse the behaviour, the hopping rate is plotted in an Arrhenius plot, i.e., ln(h) vs. 1/T, in Figure 4e. The data show a linear dependence, consistent with the Arrhenius equation for surface diffusion, $h(T) = A_m \exp[-E_m/(k_B T)]$ [47, 49, 66]. The slope of the linear fit in Figure 4e yields the migration barrier for diffusion of 2HTPP on Cu(111), $E_m = 0.71 \pm 0.08$ eV. From the ordinate intercept the preexponential factor is determined to $A_m = 10^{10.9 \pm 1.4}$ s^{-1}. These values are to be compared with the values of $E_m = 0.96 \pm 0.09$ eV and $A_m = 10^{12.0 \pm 1.4}$ s^{-1} for 2HTPyP on Cu(111) reported by Eichberger et al.[33]. The larger migration barrier is attributed to an additional interaction of the nitrogen atoms in the pyridyl side groups of 2HTPyP with the Cu substrate. Overall, it thus can be concluded that the contribution from the iminic nitrogen atoms dominates the diffusion

behaviour. Eichberger et al. report also another interesting observation, that is, a strongly enhanced mobility of 2HTPyP dimers; these dimers are presumably formed by a linkage of two 2HTPyP molecules via a Cu atom, connecting the nitrogen atoms in the pyridyl groups. The Arrhenius analysis for the diffusion of the dimers yielded E_m = 0.94 ± 0.03 eV and A_m = $10^{14.0 \pm 0.5}$ s^{-1}. Since the activation energies, E_m, for monomer and dimer diffusion are identical in the margin of error, the much higher mobility of the dimer is solely related to the higher preexponential factor and thus (as discussed in the introduction) must be due to entropic effects. This observation was attributed to the fact that upon dimer formation the TPyP internal degrees of freedom (energetically low lying bending and rocking modes) are constrained as compared to the individual molecule[33]. This nice example convincingly demonstrates that entropic effects can play an important role for activated processes.

In a next step, the temperature-dependence of the rotation of the migration direction by ± 120° is analysed between 305 and 330 K (at lower T, there are too few events for a reliable statistical analysis). The corresponding Arrhenius plot for the rotation rate $r(T) = A_r \exp[-E_r/(k_B T)]$ in Figure 4f shows again a linear behaviour, and the corresponding fit yields a rotation activation barrier of E_r = 1.28 ± 0.12 eV and a preexponential factor of $A_r = 10^{17.0 \pm 1.8}$ s^{-1}. The much higher barrier for rotation than for unidirectional motion is attributed to the very pronounced site-specificity of the N-Cu interaction, in combination with a complex change of the molecular conformation during the rotation event. If one interprets the preexponential factor of the rotation literally as a frequency factor and thus as the frequency of the molecular vibration (frustrated rotation), the corresponding value appears to be unreasonable high at first glance. However, when considering that the preexponential factor reflects the entropy gain from the initial to the transition state, one could speculate that additional degrees of freedom (e.g., nearly free azimuthal rotation in the transition state) could account for the observed high value. Indeed, for the desorption of "large" organic molecules (comparable to 2HTPP), similar and even higher frequency factors were reported in literature[67-70]. A more detailed discussion of such effects follows in Section 4.

Prior to the results just mentioned, rotational hopping of porphyrins was found only when the molecules are embedded in a closely packed supramolecular framework, at temperatures well below 100 K. Examples are zinc-octaethylporphyrin on Cu(111) with an rotational activation energy of 0.17 eV [71] and zinc-tetrakis¬(di-tert-butylphenyl)porphyrin with an activation energy of 0.24 eV [24]. Since for both metal complexes all nitrogen atoms coordinate to the central Zn ion, no pronounced site-specificity, as found for 2HTPP, is expected. Consequently, the rotational dynamics of both metalloporphyrins should be governed by lateral molecule-molecule interactions rather than by molecule-substrate interactions[33, 72]. Thus, 2HTPP on Cu(111) represents the first example for the rotation of individual porphyrin molecules on a pristine surface and for the evaluation of the corresponding rotation barrier. The results described in this section demonstrate that the investigated system is especially suitable for dynamic STM studies, owing to the fact that the pronounced site-specifity of the adsorbate-substrate interaction of 2HTPP on Cu(111) yields a untypically large surface corrugation. This allowed us to directly trace the dynamics of individual molecules at room temperature. This peculiar behaviour is in contrast to the high mobility of corresponding metalloporpyhrins, e.g., CoTPP or CuTPP, and will enable us to investigate the kinetics of a surface-confined metalation reaction in the next chapter.

3 Self-metalation of 2HTPP with Cu substrate atoms

With the first observation of surface-mediated *in situ* metalation of porphyrins a new route for the controlled fabrication of functional molecular architectures has been established[62, 73, 74], which stimulated significant further research activities[4, 32, 35, 36, 56, 59, 73-87]. It is nowadays well established that metalloporphyrins can be synthesised readily on a metal surface by the reaction of a corresponding free base porphyrin with an "available" metal atom. The respective metal atom can be provided on the surface by pre- or post-deposition, or originate from the surface itself. Depending on the metal, this in situ metalation can proceed already at room temperature or after moderate annealing[73, 74, 84]. It was studied in detail for 2HTPP with Co[4, 73, 85], Fe,[74, 84, 86, 87] Ni[56, 79], Cu[35, 36, 59, 80-83], Zn[32, 77, 78] and Ce[75, 76] on Cu(111), Ag(111) and Au(111). The surface-mediated reaction follows the equation:

$$M(ads) + 2HTPP(ads) \rightarrow MTPP(ads) + H_2(g)$$

with M being the corresponding metal. Presently, no theoretical calculations for this surface reaction are available. In gas phase DFT calculations, the reaction comprises the following elementary steps: a) coordination of the metal atom by the intact free-base porphyrin, 2HTPP, b) successive transfer of the two hydrogen atoms from the respective nitrogen atoms to the metal atom and c) formation and release of H_2. Thereby, the transfer of the first hydrogen to the metal was identified as the rate limiting step, which determines the activation energy for the metalation[83, 85]. On the surface, the situation may be more complex.

A particularly interesting surface-mediated reaction is the so called self-metalation of free base porphyrins, in which the porphyrin is metalated with a substrate atom of a metal[35, 36, 59, 80-83]. As discussed in the last section, the adsorption behaviour of 2HTPP and metalloporphyrins (e.g., CoTPP), is very different, see Figure 2. When studying the self-metalation of 2HTPP on Cu(111), this different behaviour makes it possible to discriminate the reactant 2HTPP from the reaction product CuTPP. As schematically illustrated in Figures 5a and 5b, the reactant 2HTPP is comparably immobile while the product CuTPP diffuses very fast (indicated by the horizontal arrows). As a result, CuTPPs cannot be imaged as isolated molecules in STM at room temperature. For low coverage, they can be regarded as 2D gas, and are therefore imaged only as noisy

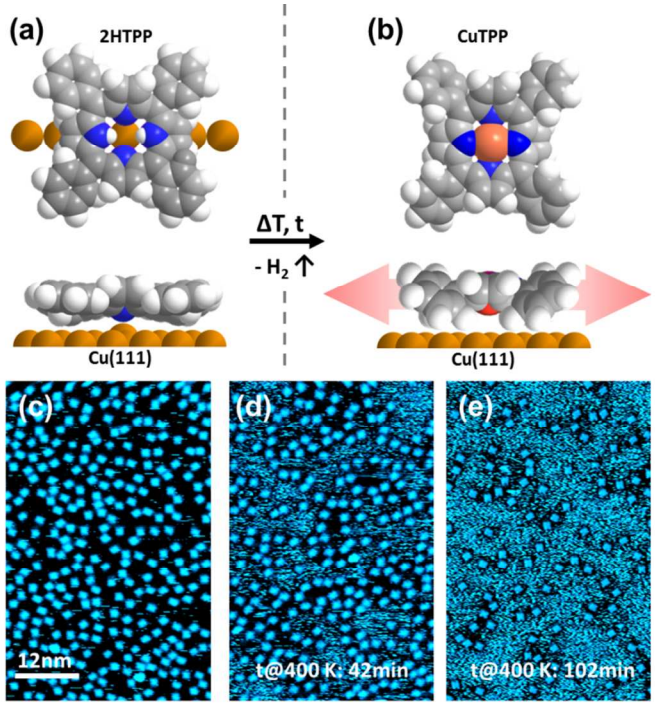

Figure 5 (a) Due to a strong interaction of the iminic nitrogen atoms of the 2HTPP porphyrin macrocycle with the underlying Cu substrate the molecule is literally pulled towards the surface, thus exhibits a flat conformation and is rather immobile at RT. (b) For CuTPP all four nitrogen atoms are coordinated equally to the Cu center. As a result the interaction with the surface is reduced and the molecule is very mobile at RT. (c)-(e) Constant current room temperature STM images of (a) 2HTPP as prepared on Cu(111) and (b), (c) after annealing to 400 K for the indicated times. The estimated molecular densities of 2HTPP and the corresponding tunnelling parameters are: (a) ρ_0= 0.135 molecules/nm^2 U= -1.07 V, I=200 pA; (b) ρ_{42min}@400K= 0.094 molecules/nm^2, U= -1.20 V, I=231 pA; (c) ρ_{102min}@400K= 0.042 molecules/nm^2, U= -1.20 V, I=230 pA. (Adapted with permission from Ditze et al. [35]. Copyright 2012 Wiley)

regions, in contrast to the 2HTPPs, which are imaged as individual molecules. The self-metalation reaction of 2HTPP on Cu(111) does not occur at RT but can be thermally activated around 400 K. In Figure 5c, an STM image of a 2HTPP layer with a coverage of ρ_0 = 0.135 molecules/nm^2 is shown after adsorption at RT. Figures 5d and 5e show the same layer after annealing to 400 K for 42 and 102 min, respectively, and subsequent cooling to RT. Clearly, a pronounced decrease of the 2HTPP density is observed with increasing annealing time. Obviously, at 400 K, the metalation reaction is slow enough to be followed on the time scale of minutes. From Figures 5c-5e is also evident that individual 2HTPP molecules are clearly distinguishable, which allows to determine their molecular density and thus to quantitatively follow the isothermal reaction as a function of time. These data measured at different temperatures then provide access to the kinetics of the reaction. The decrease of the 2HTPP density is directly related to the consumption of the reactant in the metalation reaction. In

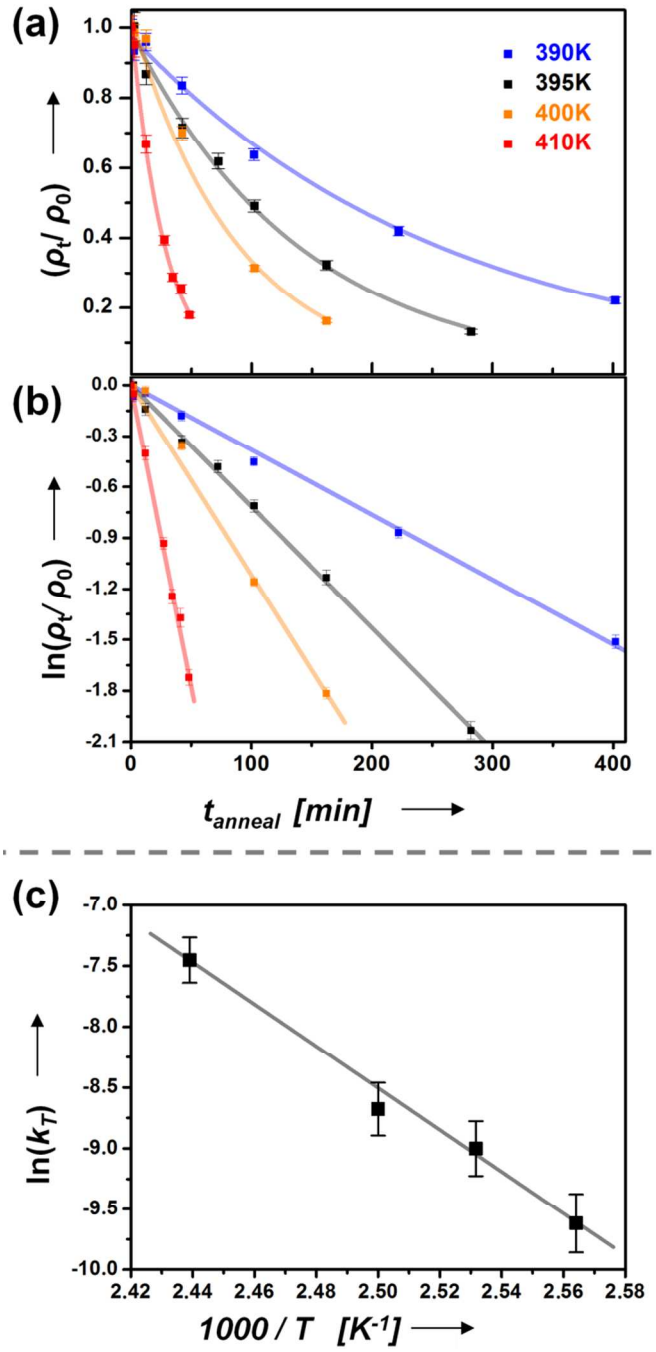

Figure 6 Graph of normalized molecular density (ρ_t/ρ_0) of 2HTPP on Cu(111) with annealing time at the indicated constant temperatures. (b) Logarithmic plot of the data in (a). (c) Arrhenius plot of the rate constants, k_T, derived from the corresponding line slopes in (b). (Reprinted with permission from Ditze et al. [35]. Copyright 2012 Wiley)

Figure 6a, the normalized 2HTPP density, ρ_t/ρ_0, is plotted as a function of time for four different temperatures, 390, 395, 400 and 410 K. The data show that, as expected, the density decreases with reaction time at a given temperature, and that the reaction proceeds faster at higher temperatures. The decrease follows an exponential behaviour for all temperatures,

which is even more evident from the logarithmic plot in Figure 6b. This is in perfect agreement with a pseudo first order reaction, according to $\rho_t/\rho_0 = \exp(-k_T \cdot t)$. Such a behaviour is expected, since the Cu(111) crystal represents an infinite reservoir for Cu atoms, i.e., the concentration of available Cu atoms does not change, and consequently the reaction rate is proportional to the concentration of 2HTPP only. The corresponding rate constants, k_T, can be directly determined as the slopes of the fitted lines in Figure 6b. Using the Arrhenius equation, $k_T = A \cdot \exp(-E_a/k_B T)$, one then obtains the activation energy, E_a, and the preexponential factor, A, by plotting $\ln(k_T)$ vs. 1/T (Figure 6c). Linear regression yields $E_a = 1.48 \pm 0.12$ eV and $A = 10^{15\pm1.6}$ s^{-1}.

The presented analysis, which is based on the isothermal "molecule counting" in STM images obtained at different temperatures, is a unique example for the experimental determination of the reactions kinetics and the activation barrier for a surface reaction of larger organic molecules. The estimated activation energy value of $E_a = 1.48 \pm 0.12$ eV is in good agreement with previous DFT calculations of the metalation reaction of the bare free base porphyrin macrocycle with Cu in the gas phase which yielded values ranging from 1.03 to 1.60 eV, depending on the level of theory and applied basis sets[32, 85]. The only value for the activation energy of a metalation reaction reported before the work of Ditze et al.[35] was derived not from isothermal data, but from a temperature-programmed desorption (TPD) measurement of deuterium during the metalation of 2DTPP (deuterated analogue of 2HTPP) with Zn on Ag(111)[85]. Using Redhead's equation[88], the activation energy was deduced. The major weakness of the Redhead approximation is the fact that the preexponential factor k_0 cannot be determined, but has to be assumed; usually a value of 10^{-13} s^{-1} was used in the corresponding analysis.

It should be noted that for the described temperature-dependent measurements it was crucial that comparable initial coverages were used: In Figure 6, the 2HTPP starting density, ρ_0, varied between 0.135 and 0.174 molecules/nm^2 (this roughly corresponds to ~23-30% of a saturated monolayer of CuTPP on Cu(111) in a well-ordered quadratic adsorbate lattice). Indeed, it was later shown that while the metalation rate is independent of coverage up to ~0.36 molecules/nm^2, it exhibits an abrupt boost by a factor of 20 above this value[36], where the transition regime to the formation of a peculiar checkerboard 2HTPP phase occurs.[57]

Possible extensions for future studies of the kinetics of metalation reactions are to investigate the role of the crystallographic orientation of the surface or the study of stepped surfaces, in order to obtain more information on the rate-limiting step. Also, calculations including the Cu surface are highly desired. Furthermore, automated image processing routines are currently developed (see Section 4), which will speed up the analysis significantly (note that for the data plotted in Figure 6 more than 250,000 2HTPPs were counted by hand). In perspective, the kinetic analysis of isothermal STM experiments might play an important role to gain detailed quantitative insight into complex surface reactions in the future.

4 Conformational switching of porphyrin molecules

Last but not least, the thermally and tip induced conformational switching of 2H-5,10,15,20-Tetrakis-(3,5-di-tert-butyl)-phenyl-porphyrin (2HTTBPP) adsorbed on Cu(111) will be reviewed [37]. Using individual molecules or atoms as functional entities[2, 89] is certainly one of the main goals of nanotechnology with the vista to engineer functional devices. One particularly fascinating area is the application of switchable molecular building blocks in information storage[90, 91]. In order to achieve this goal, however, a detailed understanding of the adsorption behaviour of large organic molecules on well-defined surfaces is essential, which has stimulated model investigations in ultra-high vacuum. A large number of studies have been performed with scanning tunnelling microscopy (STM) at low temperatures; this method not only allows for direct imaging of the adsorbed species in real space, but also opens up the possibility to manipulate the molecular objects[20, 27, 92-97]. A variety of different switching mechanisms has been investigated. These include tautomerization of naphthalocyanine or 2H-porphyrin[19, 98], molecular cascades of CO molecules on Cu(111)[99], bond formation or cleavage in adsorbed molecules[100-102], conformational modifications in general[63, 103, 104], and specifically the trans-cis conformational changes in azobenzene[105-107].

Since the activation energies in the mentioned examples are in most of the cases rather small, the corresponding experiments are typically performed at temperatures well below 80 K, in order to prevent unwanted thermally induced activation, and also surface diffusion. The applied low temperatures are certainly not compatible with "real world" applications. To engineer devices suitable for higher temperatures, new molecular building blocks have to be designed and evaluated, and a fundamental understanding of the involved mechanisms is necessary. One promising approach in this context is addressing individual molecules within a self-assembled supramolecular array with a high degree of long range order. In such an arrangement, diffusion can be effectively prevented, and one could envisage tailoring the stability of a certain molecular conformation by the interplay between adsorbate-substrate and adsorbate-adsorbate interactions. Very recently, Ditze et al. discovered that 2HTTBPP on Cu(111) is a system which fulfils these criteria[37]. 2HTTBPP is a porphyrin very similar to 2HTPP; it is significantly larger due to the attachment of two tert-butyl groups at the 3 and 5 positions of each phenyl substituent, i.e., of altogether eight tert-butyl groups. Previous studies for corresponding metallo-TTBPPs reported high conformational flexibility and thus switching capabilities on different substrates[21, 103, 104, 108, 109]. On the other hand, the uncoordinated iminic nitrogen atoms of free base porphyrins like 2HTTBPP are expected to form a strong attractive interaction with the Cu substrate[33, 81, 82]; this type of interactions were already discussed in the previous sections for the smaller 2HTPP[34-36, 58, 80, 110].

The investigation by Ditze et al. indeed reveals that 2HTTBPP exhibits a very unusual and interesting adsorption

behaviour. Figure 7a shows an overview STM image of a submonolayer of 2HTTBPP on Cu(111). The molecules are arranged in domains of alternating bright and dark rows. In the high resolution STM image in Figure 7b one can distinguish two types of appearances of 2HTTBPP: the bright rows consist of molecules with a central protrusion and the dark rows of molecules with a central depression. For both types, the periphery of the molecules appears as eight bright spots, which can be assigned to the eight tert-butyl substituents arranged in four groups around the molecular centre corresponding to the four phenyl groups[21, 104, 108].

The four peripheral groups form a rectangle (indicated in green), which is identical for the two different molecular appearances. In an earlier study on TTBPPs is was shown that the intramolecular conformation of the molecules can be deduced from the geometry of the rectangle, that is, from the aspect ratio of the short and long sides, and the perimeter[108]. The resulting conformation is described by twisting (by a twist angle θ) and/or tilting of the phenyl rings (by a tilt angle □) with respect to the porphyrin plane; see [37, 108] for details.

From the image in Figure 7b, the two angles are estimated to θ = 5 ± 5° and □ = 35 ± 5° for both conformations. The value of θ being close to zero is confirmed by the fact that all eight tert-butyl substituents appear with similar apparent height. In a recent gas phase DFT study of the energy surface of the very similar porphyrin CoTTBPP, a local minimum was found at very similar twist and tilt angles (θ = 10° and □ = 30°), albeit at a relatively high energy[109]. In this conformation the molecule adopts a concave, bowl-like shape. Such conformations, which are rather exotic and energetically unfavourable in the gas-phase, might be stabilized on a surface by molecule-substrate, but also by lateral molecule-molecule interactions. Based on these considerations, the two different appearances of 2HTTBPP on Cu(111) can be understood: the dark molecules are in a concave conformation, i.e., with the bottom of the "bowl" on the surface (Figure 7d), while the bright molecules are in a convex conformation, i.e., the bowl is upside down (Figure 7c). This interpretation was fully confirmed by DFT level simulated STM images of the molecules on a three layer Cu slab[37].

It is interesting to compare this pronounced bimodal appearance with the behaviour of two closely related systems, namely 2HTTBPP on Ag(111)[111] and CuTTBPP on Cu(111); for the latter a very different geometry (θ = 75 ± 5° and □ = 0 ± 5°) is found, which is very similar to the overall minimum reported for CoTTBPP in the gas phase calculations[109]. The very different behaviour found here for 2HTTBPP on Cu(111) (θ = 5 ± 5° and □ = 35 ± 5°) is a strong indication for considerable stabilizing interactions. For the concave conformation, this interpretation is in line with a strong attractive interaction between the iminic nitrogen atoms and the Cu substrate, by which the porphyrin macrocycle is literally "pulled" towards the surface[34, 35, 53, 55, 80]; the reason for the concave conformation, however, is not readily accessible. Here lateral interactions also must play a role and it will be later discussed that this conformation is entropically stabilized.

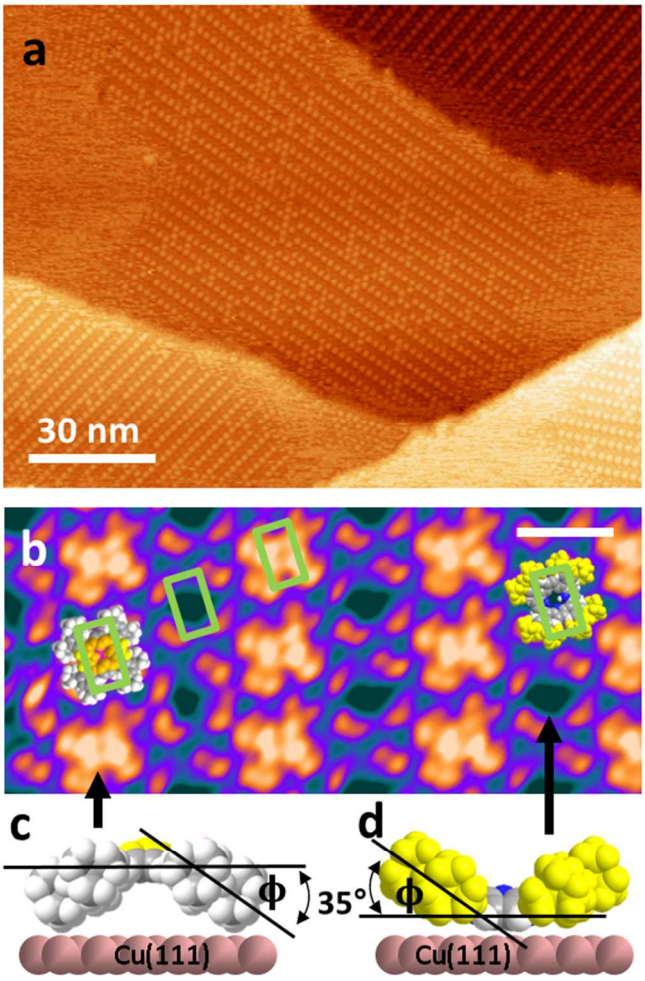

Figure 7 (a) STM image of ordered domains of 2HTTBPP on Cu(111) acquired at room temperature (U = +1.31 V, I = 30 pA). The molecules exhibit a bimodal appearance, i.e., alternating bright and dark lines/rows are visible in STM.. (b) High resolution RT STM image (U = +1.30 V, I = 30 pA) of the supramolecular order shown in a. The bright and dark rows in (a) consist of molecules with different intramolecular conformations, as indicated by the overlaid scaled models (top view). The scale bar represents 2 nm. (c, d) Space filling models of the convex (c) and concave (d) conformations of 2HTTBPP. The determination of the intramolecular conformation is based on the appearance in STM, in particular on the green rectangle formed by the peripheral substituents as indicated in the high resolution ST micrographs. (Adapted with permission from Ditze et al.[37]. Copyright 2014 American Chemical Society)

While the static situation is already peculiar, the dynamic behaviour is even more interesting. From Figure 7a, it is evident that the order in the dark and bright rows is not perfect. Indeed, inspection of successive STM images of the same surface region at RT shows that individual molecules in both rows occasionally change their appearance from dark to bright and vice versa; for better illustration, in Figure 8a a corresponding image series is shown that was extracted from a high resolution RT STM movie; switching molecules are

indicated by the white arrows (see SI Movie M1 from reference [37]). The observed behaviour demonstrates a spontaneous reversible conformational switching of individual 2HTTBPPs, indicating the metastable nature of the intramolecular conformation at room temperature.

The switching of the molecules between the two conformations in the two rows is attributed to a thermally induced process. By performing measurements at different temperatures, one can then obtain access to the corresponding temperature-dependent dynamics close to RT, and thereby obtain an understanding of the energetics of the switching. To cover a sufficient temperature range, the measurement time per image has to be comparably short. For the ST micrographs in Figure 8, the acquisition speed (15 seconds for 12 nm^2 acquired with 512^2 pixels) was not sufficient to track all switching events at RT.

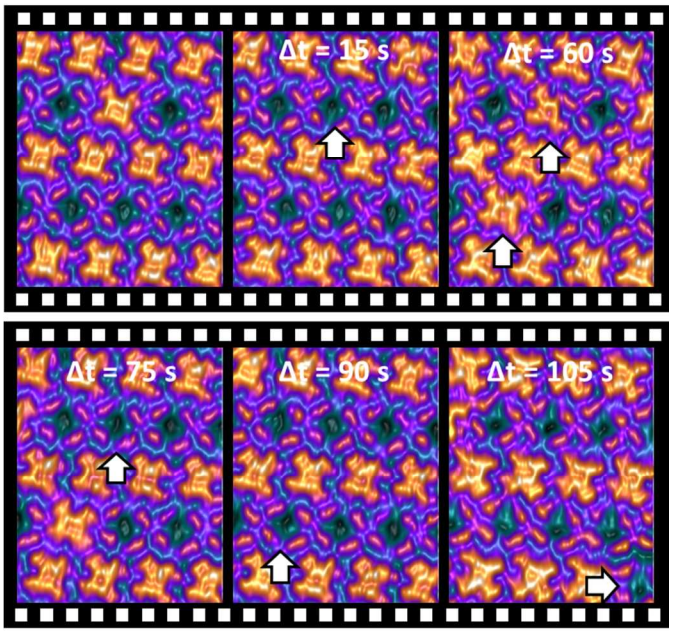

Figure 8 Selected images from a high resolution STM movie of a 2HTTBPP domain on Cu(111) acquired at RT (image to image acquisition time 15 s; U = +1.76 V, I = 24 pA). The arrows indicate individual molecules which exhibit a spontaneous conformational switching from concave to convex or *vice versa*. The times after acquisition of the first micrograph (left) are indicated by the *t* values. (Adapted with permission from Ditze et al.[37]. Copyright 2014 American Chemical Society)

In order to significantly improve the time resolution, the acquisition time for a 12 nm^2 image was reduced from 15 to 1.8 seconds, by reducing the resolution from 512^2 to 128^2 and increasing the scan speed. Even though the spatial resolution of these images is significantly lower, the contrast between concave and convex molecules is still very good[37].

Using this accelerated data acquisition, time lapse movies were measured between 270 and 320 K, and a specific visualization technique to analyse the time evolution of height profiles was applied[36]. The data show an increase of the switching rate with increasing temperature for both rows, indicative of activated processes. However, when comparing the behaviour in the two rows, it was found that molecules in the concave rows switch much more frequently than the those in the convex rows[37]. This is unexpected, since the strong attractive interaction of the iminic nitrogen of the 2HTTBPP with the substrate and significant van der Waals forces[37] suggests a stronger bond and thus a higher energy barrier for switching molecules in the concave row than in the convex row.

Further insight into these thermally driven switching processes is achieved from a quantitative analysis of isothermal time lapse movies, which were acquired at five temperatures between 280 and 300 K. The criterion for upper limit of 300 K was that the observed switching processes are still slower than the time resolution of ~1.8 s of STM for one frame to ensure that no switching events are missed. The criterion for the lower limit of 280 K was that at lower temperatures the number of switching events was not sufficient for a conclusive analysis. In recorded STM images, switching events from the "native" state to the "deviant" state and back, in both the concave and the convex rows, could be identified. In other words, four different switching events were separately analysed, namely from convex (native state) to concave and back in the bright row, and from concave (native state) to convex and back in the bright row. For this analysis, a semi-automatic image processing tool for STM movies was developed and applied. With this tool more than 1.5 million molecular conformations, from more than 70,000 STM images, were extracted from the movies at different temperatures, yielding more than 10,000 switching events. The switching rates, *r*, for the four states were determined as the number of switching events for a particular state divided by the lifetime of this state (see SI of reference [37] for details). The increase of the switching rates for all four switching events with temperature indicates that the intramolecular conformation changes are activated processes. As performed in Sections 2 and 3, such activated processes are typically evaluated with an Arrhenius analysis, which yields the activation energy *E* and the corresponding preexponential factor *A*. As already discussed in the Sections 1 and 2, the drawback of this analysis is that it does not provide direct physical insight into the nature of the preexponential factor. This insight is, however, of particular interest and relevance when major changes in the entropy of the different states occur, as is the case for the system studied here. As already outlined in Section 1, the alternative approach is based on the transition state theory (TST), where the Gibbs energy defines the activation barrier to be overcome[39]. Following a method described in detail by Winzor et al[112], one uses the logarithmic form of the Eyring equation (see Section 1) divided by T:

$$\ln\left(\frac{r}{T}\right) = \ln\left(\frac{k_B}{h}\right) + \frac{\Delta S^{\#}}{k_B} - \frac{\Delta H^{\#}}{k_B T} \quad .$$

By plotting ln*(r/T)* as a function of *1/T*, one can then extract the slope

$$m = -\frac{\Delta H^{\#}}{k_B}$$

and the ordinate intercept

$$y = \ln\left(\frac{k_B}{h}\right) + \frac{\Delta S^{\#}}{k_B}$$

With this analysis, it is possible to directly extract the values for $\Delta H^{\#}$ and $\Delta S^{\#}$. It should be noted that for simplicity the transmission factor κ was not considered here, since it is usually set to $\kappa = 1$ and makes no contribution in the logarithmic form, as $\ln(\kappa)=0$[37, 112].

In Figure 9, the corresponding plots are shown for the switching events in the concave rows (left) and the convex rows (right), as derived from the isothermal STM measurements. For both rows, the data for switching from the concave to the convex conformation and *vice versa* are shown. The lines represent the least square fits; furthermore, the resulting values for $\Delta H^{\#}$ and $\Delta S^{\#}$ are given.

The comparison of the behaviour for the two rows in Figure 9 shows that the enthalpic barriers for the transition from concave to convex (in red) are the same within the margin of errors ($\Delta H^{\#} = 0.92 \pm 0.10$ for the convex row vs. 0.99 ± 0.04 eV for the concave row). The same holds for the reverse switching direction, *i.e.,* from convex to concave (0.76 ± 0.11 vs. 0.72 ± 0.04 eV; in blue). In other words, the enthalpic barrier, $\Delta H^{\#}$, is the same for the same transition in the two different rows. The observation that the enthalpic barrier for switching from concave to convex (red) is ~30% higher than for the opposite direction (blue) can be understood, considering the strong attractive interaction of the concave molecule with the substrate. Interestingly and at first sight unexpectedly, despite this stronger interaction, the switching frequency in the concave row is larger than in the concave row; this effect is assigned to entropic contributions.

In Fig. 10, the Gibbs energy scheme, with the derived thermodynamic potentials, $\Delta H^{\#}$ (green), $T\Delta S^{\#}$ (purple) and the resulting barrier $\Delta G^{\#}$ (black), is sketched for 300 K. According to the Gibbs-Helmholtz equation, $\Delta S^{\#}$ contributes to $\Delta G^{\#}$ as $-T\Delta S^{\#}$; thus positive entropy differences lead to a lower Gibbs energy barrier in Fig. 10. We first analyse the behaviour for the convex row (Figure 10, right). If one only considers $\Delta H^{\#}$ (green), the concave conformation (yellow) would be clearly favoured, which is expected from the stronger binding to the surface. However, when including the entropic contribution $-T\Delta S^{\#}$ (violet) to the Gibbs energy the convex state becomes favourable (black). This analysis demonstrates that at 300 K convex molecules in the convex rows and thus the whole supramolecular arrangement are entropically stabilized. When analysing the behaviour in the concave row (Figure 10, left), the entropic contributions also lead to some destabilization of the enthalpically favoured concave conformation (green), but do not reverse the stability in terms of the Gibbs energy (black).

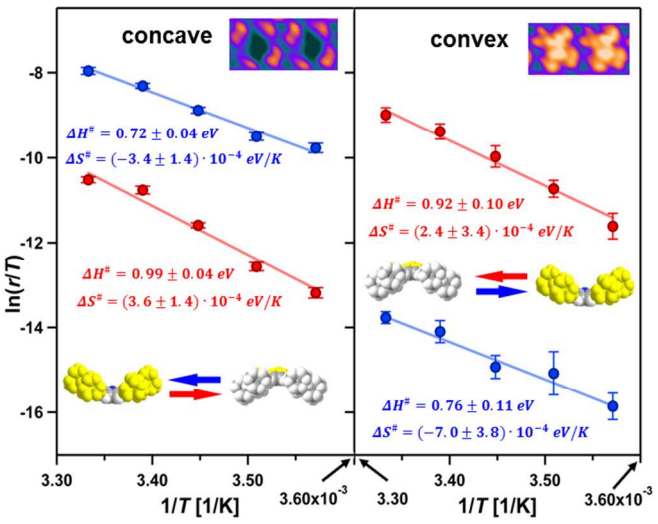

Figure 9 Plots of ln(*r*/*T*) vs. 1/*T* for the two switching events (concave to convex in red, and convex to concave in blue) in the concave row (left-hand side) and in the convex row (right-hand side). The corresponding $\Delta H^{\#}$ and $\Delta S^{\#}$ values determined from linear regressions are given in the same color code. The error bars represent the standard error. (Adapted with permission from Ditze et al.[37]. Copyright 2014 American Chemical Society)

As next step, we discuss STM results acquired at 200 K. At this temperature, no thermally induced switching between the concave and convex conformations is observed. Nevertheless, the situation is not static: STM movies measured at 200 K reveal that, irrespective of their molecular neighbourhood, convex 2HTTBPP molecules frequently change their appearance and azimuthal orientation. These observations indicate that the molecules can rotate around the surface normal already at 200 K, and that vibrational degrees of freedom and also frustrated translations are excited. In contrast, concave molecules do not change their appearance, which is attributed to the stronger molecule-substrate interaction *via* the iminic nitrogen atoms. This strong interaction not only suppresses rotational motion, but may also result in an enhanced lateral confinement, and possibly also to energetically less accessible vibrational motions due to a stiffening of the whole molecule. Thus, for the convex molecules the entropic contributions of rotational, vibrational, and frustrated translational motions are larger than those for their concave counterparts.

The influence of rotational entropy on the behaviour of larger organic molecules was recently studied by temperature programmed desorption experiments, partially combined with STM[68, 113-115]. Waldmann et al. observed large differences in the preexponential factor for desorption, depending on the rotational state before desorption[115]: the entropy difference between adsorbed molecules and desorbed molecules in the gas phase was found to be smaller for molecules, which rotate in the adsorbed state, as compared to non-rotating ones. To obtain an estimate for the here studied systems, we follow the route described by Waldmann et al. [115]; for the rotational entropy of a 2HTTBPP molecule freely rotating around an axis

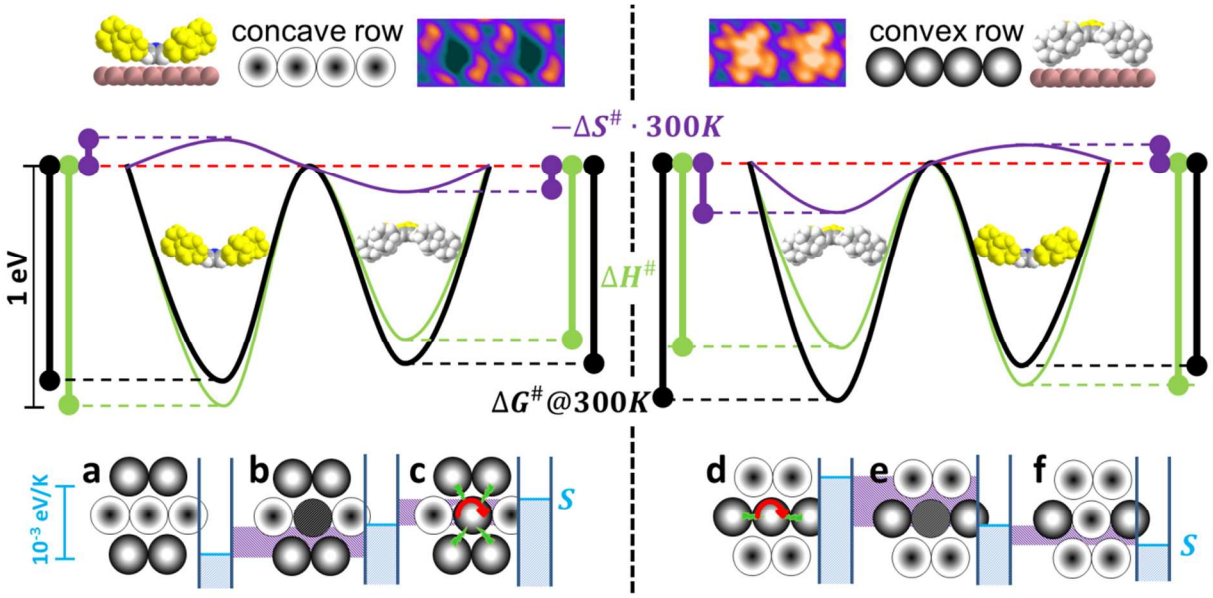

Figure 10 Sketch of the thermodynamic potential differences at 300 K (vertical bars) and the resulting energy landscape for conformational switching of 2HTTBPP on Cu(111) in the concave (left side) and the convex row (right side). The curve, which determines the switching behaviour, is the one for $\Delta G^{\#}$ drawn in black. The free energy difference is composed of contributions from $\Delta H^{\#}$ and $-\Delta S^{\#} \cdot 300$ K, displayed in green and purple, respectively. Please note that by reducing the temperature the free energy value will shift towards the enthalpy value, *i.e.,* at 0 *K* the black curve coincides with the green one. In the bottom row, schematics of the central molecule in the convex (c, d: central bright spot), the transition state (b, e: black) and the concave conformation (a, f: central dark spot), along with their next neighbors, are depicted. The height of the blue bar indicates the entropy values *S*, and the purple bars mark the corresponding entropy differences $\Delta S^{\#} \cdot$as extracted from the data depicted in Fig. 4 and directly related to the $-\Delta S^{\#} \cdot 300$ K values above (also printed in purple). The observed entropy increase from concave over the transition state to convex can be explained by the strong molecule-substrate interaction in the concave conformation going along with reduced degrees of freedom. Exemplarily, the rotation of convex molecules is indicated by the red arrows in the scheme (c, d); the green flashes (c, d) indicate steric hindrance by next neighbor molecules with the same convex conformation and thus reduced rotation, *i.e.* smaller entropy. (Reprinted with permission from Ditze et al.[37]. Copyright 2014 American Chemical Society)

perpendicular to the surface plane this yields a value of $5.1 \cdot 10^{-4}$ eV K^{-1}. This corresponds to a $T\Delta S^{\#}$ value of 0.15 eV at 300 K, and represents the difference between a freely rotating and a non-rotating 2HTTBPP. This certainly has to be considered only as an upper estimate for the actual value, since in the supramolecular structure the convex molecule is not expected to rotate freely. This value is to be compared with the $T\Delta S^{\#}$ difference of 0.28 eV at 300 K, deduced from the entropy difference of the two conformations for the convex row in Figure 9 (right). The rotational entropy value of 0.15 eV is only ~55% of the measured value. We attribute this difference to the fact also other degrees of freedom, that is, vibrations and frustrated translations, will contribute to entropy difference between the two conformations.

In the following analysis, we exemplarily focus on the rotation to obtain a qualitative picture of the entropy differences. The bottom part of Figure 10 schematically illustrates the explanation for the entropy differences by considering one specific molecule (in the center) with its six next neighbours. Our conjecture is that the more strongly bound concave molecules (a, f) generally have much smaller entropy than the convex ones (c, d), which are able to rotate supramolecular structure (indicated by red arrows). Thereby neighbouring molecules can be considered as "bearing" for the rotational motion [116]. From our data and simple steric considerations we propose that neighbours with the same conformation hinder rotation, and also other motions, due to steric repulsions. Hence, for a convex molecule, with increasing number of convex next neighbours (indicated with green flashes in c, d) the degree of freedom of rotational motion will be increasingly frustrated and thus the entropy will decrease. In other words, the rotational entropy of a convex molecule with convex neighbours in the neighbouring rows (c) is lower than that of a convex molecule which has only two convex neighbours (d). Based on these considerations, i.e., by accounting for the conformation of the central molecules and its neighbours, the relative magnitude of the entropies from Figure 9 (indicated by the blue horizontal bars at the right side of the structures) can be understood (a)-(f).

In addition to the detailed analysis of thermally induced switching close to RT, Ditze et al. also demonstrated the intentional switching of selected individual porphyrin molecules with the STM tip at 200 K; at this temperature, thermally induced switching is completely suppressed[37].

Interestingly, only convex molecules could be switched to the concave conformation, by applying bias pulses (e.g., +1.75 V for 5 seconds with closed feedback loop maintaining I= 30 pA) while the reverse process was not possible. This behaviour can partly be understood considering that the entropic contributions to the activation barrier decrease with temperature, and thus the energy landscape of the free energy (black in Figure 10) will shift towards the enthalpy contribution (green in Fig. 10) until both curves merge at 0 K. In other words, both the entropic stabilization of the convex conformation and the entropic destabilization of the concave conformation decrease with decreasing temperature. Thus, at lower temperatures, the concave conformation becomes increasingly favourable also in the convex row. As a consequence, the free energy barrier for switching from convex to concave is reduced and thus the corresponding tip-induced switching is facilitated. Apart from this thermodynamic argument, one also has to consider that tip-induced switching results from the impact of the tunnelling electron. Therefore, the cross sections for inelastic electron excitations or relaxation channels for exited states in the molecule will play an important role. With respect to the latter, the strong coupling of the concave molecules to the substrate could provide an effective decay channel for tip-induced excitations, which leads to a quenching of the switching from concave to the convex conformation.

At last point, it is interesting to note that consecutive switching of directly neighbouring molecules in a convex row leads to the destruction of the local supramolecular order. However, switching every second molecule in the convex row leaves the supramolecular arrangement intact. Thus, a maximum information storage density of $4.9 \cdot 10^{13}$ bit/inch^2 can be achieved with 2HTTBPP on Cu(111).

To conclude this section, the presented example not only provides detailed insights in thermally induced switching and the role of entropic effects, but it also underlines the potential and importance of corresponding RT measurements, in particular for systems with energetic landscapes that have the potential for room temperature applications. Furthermore, the results also considerably expand the field of STM tip-induced molecular switching to higher temperatures, which is a crucial and important step towards devices for room temperature applications.

5 Conclusions and outlook

In this feature, three different case studies were reviewed which, based on isothermal STM measurements in UHV, provide insight into the dynamics of diffusion, reactions and molecular switching at surfaces. The reviewed examples demonstrate that variable temperature STM can be a suitable tool to directly monitor the dynamic behaviour of individual adsorbed molecules, at and close to room temperature. In all cases, the behaviour of the free-base porphyrins 2HTPP and 2HTTBPP on Cu(111) was investigated. These systems proved to be particularly suitable for such studies, due to the strong bonding interaction of the iminic nitrogen atoms in the porphyrin macrocycle with the Cu substrate atoms. As a consequence, the corresponding activation energies for diffusion, reaction and switching are of a magnitude that allows following the processes around room temperature, in contrast to most previous studies, which were performed at cryogenic temperatures.

The first example addressed the surface diffusion of 2HTPP on Cu(111). For this system, individual isolated 2HTPP molecules can be observed by standard STM at RT and their migration on the surface can be traced accurately. This gives access to temperature-dependent measurements of the dynamic behaviour at and close to RT, namely diffusion and rotation. Using an Arrhenius analysis, the activation barrier for migration was determined to $E_m = 0.71 \pm 0.08$ eV, with a preexponential factor $A_m = 10^{10.9 \pm 1.4}$ s^{-1}. In an analogous way the activation barrier for the rotation of the migration direction by ± 120° was determined to $E_r = 1.28 \pm 0.12$ eV, with an preexponential factor of $A_r = 10^{17.0 \pm 1.8}$ s^{-1}. The adsorption behaviour is strongly modified if a metal center is complexed in the porphyrin macrocycle, coordinated to all four nitrogen, which considerably weakens the molecule-substrate interaction as compared to 2HTPP. Consequently, metalloporphyrins such as CuTPP or CoTPP diffuse much faster at RT such that they cannot be imaged as an isolated species anymore.

The second example dealt with the self-metalation of 2HTPP on Cu(111). By heating the sample to temperatures around 400 K, the insertion of a Cu atom into the porphyrin macrocycle, that is, the formation of CuTPP, is thermally induced. The progress of the reaction was followed by subsequent imaging the surface, and counting the remaining 2HTPPs, as a function of annealing time at the elevated temperature. By performing such measurements for different annealing temperatures between 390 and 410 K, the kinetics of the self-metalation reaction was studied. From an Arrhenius analysis, the activation energy and the preexponential factor were determined to $E_a = 1.48 \pm 0.12$ eV and $A = 10^{15 \pm 1.6}$ s^{-1}, respectively

In the third example, we reviewed the thermally induced conformational switching of 2HTTBPP on Cu(111). Upon adsorption at room temperature, 2HTTBPPs self-assemble in a long-range ordered structure, with a bimodal appearance in STM. This specific structure is attributed to alternating rows of molecules with concave and convex intramolecular conformation. For both rows, switching between the concave and convex conformation is observed around room temperature. In order to study the energetics of this thermally induced switching process, temperature-dependent measurements were performed between 280 and 300 K. The analysis of the corresponding kinetic data for this example was not performed using an Arrhenius analysis, but in the framework of transition state theory, based on the Eyring equation. From this analysis of the free energy landscape, a more detailed insight in interpretable thermodynamic potentials can be obtained. In particular, the entropy gain and the enthalpic barrier for the different switching processes were determined. The extracted

values evidence a dominating role of entropic effects in the system at room temperature. In the alternative Arrhenius analysis such entropic effects find their analogue in differences in the preexponential factors. These can also be transformed into the corresponding entropy values, as shown by Eichberger et al., when investigating an unexpectedly fast surface of 2HTPyP dimers on Cu(111)[33].

As an outlook, we want to stress the importance of the results by Buchner et al.[34], Eichberger et al.[33] and Ditze et al.[37] achieved by UHV STM, which demonstrate that entropic effects have to be generally considered for large organic molecules on surfaces at and close to RT. The general character of these investigations is underlined by recent STM experiments at the liquid/solid interface. Friesen et al. investigated the dynamics of reversible binding of O_2 at the metal centre of cobaltoctaethylporphyrin[117], and Blunt et al. studied the dynamics of reversible transformation of two supramolecular phases of an alkylated dehydrobenzo[12]-annulene derivative[118] in solution on an HOPG surface. In temperature- and concentration-dependent STM studies, the entropic and enthalpic contributions were estimated and the authors also report significant contributions from entropy close to RT[117, 118]. Overall; the discussed examples clearly indicate the necessity to further investigate fundamental questions concerning the role of the thermodynamic potentials, in particular of entropic effects, in such processes. From an application point, there is an urgent need to further explore supramolecular systems with specifically tailored organic molecules at RT, in order to evaluate their potential as functional building blocks in room temperature applications. Here, strong collaborations with synthetic chemistry and theory are required, in order to tailor molecules that are suitable, e.g., for switching at and preferably even above room temperature.

Acknowledgements

The authors gratefully acknowledge the funding of the German Research Council (DFG) by the Collaborative Research Center 583 and by the Cluster of Excellence 'Engineering of Advanced Materials' (http://www.eam.uni-erlangen.de) at the Universität Erlangen-Nürnberg. They are also very grateful to their former and present coworkers and students, Dr. F. Buchner, Dr. S. Ditze, F. Stark, Dr. K. Comanici, E. Zillner, M. Drost, M. Röckert, Dr. J. Xiao, M. Chen, Dr. O. Lytken, Prof. J. M. Gottfried, Nicola Luckas, Dr. W. Hieringer, Prof. A. Görling, Prof. N. Jux, André Aichert and Prof. J. Hornegger, for their excellent work and the fruitful collaboration.

Notes and references

[a] Lehrstuhl für Physikalische Chemie II, Egerlandstrasse 3 and Interdisciplinary Center for Molecular Materials (ICMM), Universität Erlangen-Nürnberg, D-91058 Erlangen, Germany.

1. G. Binnig, H. Rohrer, C. Gerber and E. Weibel, *Physical Review Letters*, 1982, **49**, 57-61.
2. J. V. Barth, G. Costantini and K. Kern, *Nature*, 2005, **437**, 671-679.
3. J. V. Barth, J. Weckesser, N. Lin, A. Dmitriev and K. Kern, *Appl. Phys. A-Mater. Sci. Process.*, 2003, **76**, 645-652.
4. J. M. Gottfried and H. Marbach, *Z. Phys. Chemie-Int. J. Res. Phys. Chem. Chem. Phys.*, 2009, **223**, 53-74.
5. L. R. Milgrom, *The Colours of Life*, Oxford University Press, 1997.
6. K. M. Kadish, K. M. Smith, R. Guilard and (Eds.), *The Porphyrin Handbook Vol. 4: Biochemistry and Binding: Activation of Small Molecules*, Academic Press, San Diego, 2000.
7. K. M. Kadish, K. M. Smith, R. Guilard and (Eds.), *The Porphyrin Handbook Vol. 13: Chlorophylls and Bilins: Biosynthesis, Synthesis, and Degradation*, Academic Press, San Diego, 2003.
8. N. A. Rakow and K. S. Suslick, *Nature*, 2000, **406**, 710-713.
9. G. Guillaud, J. Simon and J. P. Germain, *Coordination Chemistry Reviews*, 1998, **178–180**, 1433–1484.
10. S. Kang, M. Yasuda, H. Miyasaka, H. Hayashi, M. Kawasaki, T. Umeyama, Y. Matano, K. Yoshida, S. Isoda and H. Imahori, *ChemSusChem*, 2008, **1**, 254-261.
11. L. Y. Luo, C. F. Lo, C. Y. Lin, I. J. Chang and E. W. G. Diau, *Journal of Physical Chemistry B*, 2006, **110**, 410-419.
12. M. Morisaki, K. Enomoto, T. Ito, I. Tabata, K. Hisada and T. Hori, *Sen-I Gakkaishi*, 2007, **63**, 301-306.
13. L. Schmidt-Mende, W. M. Campbell, Q. Wang, K. W. Jolley, D. L. Officer, M. K. Nazeeruddin and M. Gratzel, *Chemphyschem*, 2005, **6**, 1253-1258.
14. Q. Wang, W. M. Carnpbell, E. E. Bonfantani, K. W. Jolley, D. L. Officer, P. J. Walsh, K. Gordon, R. Humphry-Baker, M. K. Nazeeruddin and M. Gratzel, *Journal of Physical Chemistry B*, 2005, **109**, 15397-15409.
15. J. H. Yum, S. R. Jang, R. Humphry-Baker, M. Gratzel, J. J. Cid, T. Torres and M. K. Nazeeruddin, *Langmuir*, 2008, **24**, 5636-5640.
16. J. V. Barth, *Annu. Rev. Phys. Chem.*, 2007, **58**, 375-407.
17. J. Otsuki, *Coordination Chemistry Reviews*, 2010, **254**, 2311-2341.
18. W. Auwärter, F. Klappenberger, A. Weber-Bargioni, A. Schiffrin, T. Strunskus, C. Wöll, Y. Pennec, A. Riemann and J. V. Barth, *J. Am. Chem. Soc.*, 2007, **129**, 11279-11285.
19. W. Auwarter, K. Seufert, F. Bischoff, D. Ecija, S. Vijayaraghavan, S. Joshi, F. Klappenberger, N. Samudrala and J. V. Barth, *Nat. Nanotechnol.*, 2012, **7**, 41-46.
20. X. H. Qiu, G. V. Nazin and W. Ho, *Science*, 2003, **299**, 542-546.
21. T. A. Jung, R. R. Schlittler and J. K. Gimzewski, *Nature*, 1997, **386**, 696-698.
22. H. Spillmann, A. Kiebele, M. Stohr, T. A. Jung, D. Bonifazi, F. Y. Cheng and F. Diederich, *Advanced Materials*, 2006, **18**, 275-+.
23. M. Stöhr, M. Wahl, H. Spillmann, L. H. Gade and T. A. Jung, *Small*, 2007, **3**, 1336-1340.
24. N. Wintjes, D. Bonifazi, F. Y. Cheng, A. Kiebele, M. Stöhr, T. Jung, H. Spillmann and F. Diederich, *Angewandte Chemie-International Edition*, 2007, **46**, 4089-4092.
25. N. Wintjes, J. Hornung, J. Lobo-Checa, T. Voigt, T. Samuely, C. Thilgen, M. Stohr, F. Diederich and T. A. Jung, *Chemistry-a European Journal*, 2008, **14**, 5794-5802.
26. L. A. Fendt, M. Stohr, N. Wintjes, M. Enache, T. A. Jung and F. Diederich, *Chemistry-a European Journal*, 2009, **15**, 11139-11150.

27. Y. F. Wang, J. Kroger, R. Berndt and W. A. Hofer, *Journal of the American Chemical Society*, 2009, **131**, 3639-3643.
28. L. Grill, K. H. Rieder, F. Moresco, G. Rapenne, S. Stojkovic, X. Bouju and C. Joachim, *Nat. Nanotechnol.*, 2007, **2**, 95-98.
29. V. Arima, R. L. R. Blyth, F. Matino, L. Chiodo, T. Della Sala, J. Thompson, T. Regier, R. Del Sole, G. Mele, G. Vasapollo, R. Cingolani and R. Rinaldi, *Small*, 2008, **4**, 497-506.
30. F. Matino, G. Schull, U. Jana, F. Kohler, R. Berndt and R. Herges, *Chemical Communications*, 2010, **46**, 6780-6782.
31. K. Flechtner, A. Kretschmann, H.-P. Steinrück and J. M. Gottfried, *J. Am. Chem. Soc.*, 2007, **129**, 12110-12111.
32. A. Kretschmann, M.-M. Walz, K. Flechtner, H.-P. Steinrück and J. M. Gottfried, *Chemical Communications*, 2007, 568-570.
33. M. Eichberger, M. Marschall, J. Reichert, A. Weber-Bargioni, W. Auwa□rter, R. L. C. Wang, H. J. Kreuzer, Y. Pennec, A. Schiffrin and J. V. Barth, *Nano Lett.*, 2008, **8**, 4608-4613.
34. F. Buchner, J. Xiao, E. Zillner, M. Chen, M. Rückert, S. Ditze, M. Stark, H.-P. Steinrück, J. M. Gottfried and H. Marbach, *J. Phys. Chem. C*, 2011, **115**, 24172.
35. S. Ditze, M. Stark, M. Drost, F. Buchner, H.-P. Steinrück and H. Marbach, *Angewandte Chemie International Edition*, 2012, **51**, 10898-10901.
36. M. Röckert, S. Ditze, M. Stark, J. Xiao, H.-P. Steinrück, H. Marbach and O. Lytken, *The Journal of Physical Chemistry C*, 2013, **118**.
37. S. Ditze, M. Stark, F. Buchner, A. Aichert, N. Jux, N. Luckas, A. Goerling, W. Hieringer, J. Hornegger, H.-P. Steinrück and H. Marbach, *Journal of the American Chemical Society*, 2014.
38. S. Arrhenius, *Zeitschrift für Physikalische Chemie*, 1889, **4**.
39. K. J. Laidler, S. Glasstone and H. Eyring, *The Journal of Chemical Physics*, 1940, **8**, 659-667.
40. S. de Feyter and F. C. de Schryver, *Chemical Society Reviews*, 2003, **32**, 139-150.
41. E. Ganz, S. K. Theiss, I.-S. Hwang and J. Golovchenko, *Physical Review Letters*, 1992, **68**, 1567-1570.
42. B. S. Swartzentruber, *Physical Review Letters*, 1996, **76**, 459-462.
43. T. Zambelli, J. Trost, J. Wintterlin and G. Ertl, *Physical Review Letters*, 1996, **76**, 795-798.
44. T. R. Linderoth, S. Horch, E. Lægsgaard, I. Stensgaard and F. Besenbacher, *Physical Review Letters*, 1997, **78**, 4978-4981.
45. J. V. Barth, H. Brune, B. Fischer, J. Weckesser and K. Kern, *Physical Review Letters*, 2000, **84**, 1732-1735.
46. F. Rosei, M. Schunack, Y. Naitoh, P. Jiang, A. Gourdon, E. Laegsgaard, I. Stensgaard, C. Joachim and F. Besenbacher, *Progress in Surface Science*, 2003, **71**, 95-146.
47. M. Schunack, T. R. Linderoth, F. Rosei, E. Lægsgaard, I. Stensgaard and F. Besenbacher, *Physical Review Letters*, 2002, **88**, 156102.
48. K.-Y. Kwon, K. L. Wong, G. Pawin, L. Bartels, S. Stolbov and T. S. Rahman, *Physical Review Letters*, 2005, **95**, 166101.
49. J. Weckesser, J. V. Barth and K. Kern, *Journal of Chemical Physics*, 1999, **110**, 5351-5354.
50. J. Weckesser, A. De Vita, J. V. Barth, C. Cai and K. Kern, *Physical Review Letters*, 2001, **8709**, art. no.-096101.
51. T. Yokoyama, T. Takahashi and K. Shinozaki, *Physical Review B*, 2010, **82**, 155414.
52. F. Buchner, I. Kellner, W. Hieringer, A. Gorling, H. P. Steinruck and H. Marbach, *Physical Chemistry Chemical Physics*, 2010, **12**, 13082-13090.
53. G. Rojas, X. Chen, C. Bravo, J.-H. Kim, J.-S. Kim, J. Xiao, P. A. Dowben, Y. Gao, X. C. Zeng, W. Choe and A. Enders, *Journal of Physical Chemistry C*, 2010, **114**, 9408-9415.
54. G. Rojas, S. Simpson, X. Chen, D. A. Kunkel, J. Nitz, J. Xiao, P. A. Dowben, E. Zurek and A. Enders, *Physical Chemistry Chemical Physics*, 2012, **14**, 4971-4976.
55. F. Buchner, E. Zillner, M. Roeckert, S. Glaessel, H.-P. Steinrueck and H. Marbach, *Chemistry-a European Journal*, 2011, **17**, 10226-10229.
56. S. Ditze, M. Röckert, F. Buchner, E. Zillner, M. Stark, H.-P. Steinrück and H. Marbach, *Nanotechnology*, 2013, **24**, 115305.
57. M. Stark, S. Ditze, M. Drost, F. Buchner, H.-P. Steinrück and H. Marbach, *Langmuir*, 2013, **29**, 4104-4110.
58. J. Xiao, S. Ditze, M. Chen, F. Buchner, M. Stark, M. Drost, H.-P. Steinru□ck, J. M. Gottfried and H. Marbach, *J. Phys. Chem. C*, 2012, **116**, 12275-12282.
59. J. Xiao, S. Ditze, M. Chen, F. Buchner, M. Stark, M. Drost, H. P. Steinruck, J. M. Gottfried and H. Marbach, *Journal of Physical Chemistry C*, 2012, **116**, 12275-12282.
60. J. Brede, M. Linares, S. Kuck, J. Schwobel, A. Scarfato, S. H. Chang, G. Hoffmann, R. Wiesendanger, R. Lensen, P. H. J. Kouwer, J. Hoogboom, A. E. Rowan, M. Broring, M. Funk, S. Stafstrom, F. Zerbetto and R. Lazzaroni, *Nanotechnology*, 2009, **20**.
61. G. Rojas, X. Chen, C. Bravo, J. H. Kim, J. S. Kim, J. Xiao, P. A. Dowben, Y. Gao, X. C. Zeng, W. Choe and A. Enders, *Journal of Physical Chemistry C*, 2010, **114**, 9408-9415.
62. F. Buchner, V. Schwald, K. Comanici, H.-P. Steinrück and H. Marbach, *ChemPhysChem*, 2007, **8**, 241-243.
63. H. Yanagi, H. Mukai, K. Ikuta, T. Shibutani, T. Kamikado, S. Yokoyama and S. Mashiko, *Nano Lett.*, 2002, **2**, 601-604.
64. S. Berner, M. Brunner, L. Ramoino, H. Suzuki, H. J. Güntherodt and T. A. Jung, *Chemical Physics Letters*, 2001, **348**, 175-181.
65. J. Weckesser, J. V. Barth and K. Kern, *Physical Review B*, 2001, **64**, 161403.
66. J. V. Barth, *Surf. Sci. Rep.*, 2000, **40**, 75-149.
67. R. Zacharia, H. Ulbricht and T. Hertel, *Physical Review B*, 2004, **69**, 155406.
68. M. Roos, A. Breitruck, H. E. Hoster and R. J. Behm, *Physical Chemistry Chemical Physics*, 2010, **12**, 818-822.
69. S. L. Tait, Z. Dohnalek, C. T. Campbell and B. D. Kay, *The Journal of Chemical Physics*, 2005, **122**, 164708-164713.
70. S. L. Tait, Z. Dohnalek, C. T. Campbell and B. D. Kay, *The Journal of Chemical Physics*, 2006, **125**, 234308.
71. M. Wahl, M. Stohr, H. Spillmann, T. A. Jung and L. H. Gade, *Chemical Communications*, 2007, 1349-1351.
72. B. G. Briner, M. Doering, H.-P. Rust and A. M. Bradshaw, *Science*, 1997, **278**, 257-260.
73. J. M. Gottfried, K. Flechtner, A. Kretschmann, T. Lukasczyk and H. P. Steinrück, *Journal of the American Chemical Society*, 2006, **128**, 5644-5645.
74. W. Auwärter, A. Weber-Bargioni, S. Brink, A. Riemann, A. Schiffrin, M. Ruben and J. V. Barth, *ChemPhysChem*, 2007, **8**, 250-254.

75. A. Weber-Bargioni, J. Reichert, A. P. Seitsonen, W. Auwärter, A. Schiffrin and J. V. Barth, *J. Phys. Chem. C*, 2008, **112**, 3453-3455.
76. D. Ecija, W. Auwarter, S. Vijayaraghavan, K. Seufert, F. Bischoff, K. Tashiro and J. V. Barth, *Angewandte Chemie-International Edition*, 2011, **50**, 3872-3877.
77. T. E. Shubina, H. Marbach, K. Flechtner, A. Kretschmann, N. Jux, F. Buchner, H.-P. Steinrück, T. Clark and J. M. Gottfried, *J. Am. Chem. Soc.*, 2007, **129**, 9476-9483.
78. K. Flechtner, A. Kretschmann, L. R. Bradshaw, M. M. Walz, H. P. Steinrück and J. M. Gottfried, *Journal of Physical Chemistry C*, 2007, **111**, 5821-5824.
79. M. Chen, X. F. Feng, L. Zhang, H. X. Ju, Q. Xu, J. F. Zhu, J. M. Gottfried, K. Ibrahim, H. J. Qian and J. O. Wang, *J. Phys. Chem. C*, 2010, **114**, 9908-9916.
80. K. Diller, F. Klappenberger, M. Marschall, K. Hermann, A. Nefedov, C. Woll and J. V. Barth, *J. Chem. Phys.*, 2012, **136**, 014705-014713.
81. R. Gonzalez-Moreno, C. Sanchez-Sanchez, M. Trelka, R. Otero, A. Cossaro, A. Verdini, L. Floreano, M. Ruiz-Bermejo, A. Garcia-Lekue, J. A. Martin-Gago and C. Rogero, *J. Phys. Chem. C*, 2011, **115**, 6849-6854.
82. S. Haq, F. Hanke, M. S. Dyer, M. Persson, P. Iavicoli, D. B. Amabilino and R. Raval, *Journal of the American Chemical Society*, 2011, **133**, 12031-12039.
83. Y. Li, J. Xiao, T. E. Shubina, M. Chen, Z. L. Shi, M. Schmid, H. P. Steinruck, J. M. Gottfried and N. Lin, *Journal of the American Chemical Society*, 2012, **134**, 6401-6408.
84. F. Buchner, V. Schwald, K. Comanici, H. P. Steinruck and H. Marbach, *Chemphyschem*, 2007, **8**, 241-243.
85. T. E. Shubina, H. Marbach, K. Flechtner, A. Kretschmann, N. Jux, F. Buchner, H. P. Steinruck, T. Clark and J. M. Gottfried, *Journal of the American Chemical Society*, 2007, **129**, 9476-9483.
86. F. Buchner, I. Kellner, H. P. Steinruck and H. Marbach, *Z. Phys. Chemie-Int. J. Res. Phys. Chem. Chem. Phys.*, 2009, **223**, 131-144.
87. F. Buchner, K. Flechtner, Y. Bai, E. Zillner, I. Kellner, H.-P. Steinrück, H. Marbach and J. M. Gottfried, *J. Phys. Chem. C*, 2008, **112**, in press.
88. P. A. Redhead, *Vacuum*, 1962, **12**, 203.
89. C. Joachim, J. K. Gimzewski and A. Aviram, *Nature*, 2000, **408**, 541-548.
90. R. L. Carroll and C. B. Gorman, *Angewandte Chemie International Edition*, 2002, **41**, 4378-4400.
91. J. E. Green, J. Wook Choi, A. Boukai, Y. Bunimovich, E. Johnston-Halperin, E. DeIonno, Y. Luo, B. A. Sheriff, K. Xu, Y. Shik Shin, H.-R. Tseng, J. F. Stoddart and J. R. Heath, *Nature*, 2007, **445**, 414-417.
92. J. S. Foster, J. E. Frommer and P. C. Arnett, *Nature*, 1988, **331**, 324-326.
93. L. Grill, *J. Phys.-Condes. Matter*, 2008, **20**.
94. W. Ho, *Journal of Chemical Physics*, 2002, **117**, 11033-11061.
95. G. V. Nazin, X. H. Qiu and W. Ho, *Science*, 2003, **302**, 77-81.
96. J. Schaffert, M. C. Cottin, A. Sonntag, H. Karacuban, C. A. Bobisch, N. Lorente, J.-P. Gauyacq and R. Moeller, *Nat. Mater.*, 2013, **12**, 223-227.
97. K. Morgenstern, *Surface and Interface Analysis*, 2010, **42**, 1634-1636.
98. P. Liljeroth, J. Repp and G. Meyer, *Science*, 2007, **317**, 1203-1206.
99. A. J. Heinrich, C. P. Lutz, J. A. Gupta and D. M. Eigler, *Science*, 2002, **298**, 1381-1387.
100. P. Maksymovych, D. C. Sorescu, K. D. Jordan and J. T. Yates, *Science*, 2008, **322**, 1664-1667.
101. F. Mohn, J. Repp, L. Gross, G. Meyer, M. S. Dyer and M. Persson, *Physical Review Letters*, 2010, **105**.
102. M. Piantek, G. Schulze, M. Koch, K. J. Franke, F. Leyssner, A. Krueger, C. Navio, J. Miguel, M. Bernien, M. Wolf, W. Kuch, P. Tegeder and J. I. Pascual, *Journal of the American Chemical Society*, 2009, **131**, 12729-12735.
103. C. Loppacher, M. Guggisberg, O. Pfeiffer, E. Meyer, M. Bammerlin, R. Luthi, R. Schlittler, J. K. Gimzewski, H. Tang and C. Joachim, *Physical Review Letters*, 2003, **90**.
104. F. Moresco, G. Meyer, K. H. Rieder, H. Tang, A. Gourdon and C. Joachim, *Physical Review Letters*, 2001, **86**, 672-675.
105. M. Alemani, M. V. Peters, S. Hecht, K.-H. Rieder, F. Moresco and L. Grill, *Journal of the American Chemical Society*, 2006, **128**, 14446-14447.
106. A. Safiei, J. Henzl and K. Morgenstern, *Physical Review Letters*, 2010, **104**.
107. M. Wolf and P. Tegeder, *Surface Science*, 2009, **603**, 1506-1517.
108. F. Buchner, K. Comanici, N. Jux, H. P. Steinrueck and H. Marbach, *Journal of Physical Chemistry C*, 2007, **111**, 13531-13538.
109. T. Wölfle, A. Görling and W. Hieringer, *Physical Chemistry Chemical Physics*, 2008, **10**, 5739-5742.
110. M. Stark, S. Ditze, M. Drost, F. Buchner, H. P. Steinruck and H. Marbach, *Langmuir*, 2013, **29**, 4104-4110.
111. F. Buchner, *STM Investigation of Molecular Architectures of Porphynoids on a Ag(111) Surface*, Springer, 2010.
112. D. J. Winzor and C. M. Jackson, *Journal of Molecular Recognition*, 2006, **19**, 389-407.
113. C. T. Campbell and J. R. V. Sellers, *Journal of the American Chemical Society*, 2012, **134**, 18109-18115.
114. K. R. Paserba and A. J. Gellman, *Physical Review Letters*, 2001, **86**, 4338-4341.
115. T. Waldmann, J. Klein, H. E. Hoster and R. J. Behm, *Chemphyschem*, 2013, **14**, 162-169.
116. J. K. Gimzewski, C. Joachim, R. R. Schlittler, V. Langlais, H. Tang and I. Johannsen, *Science*, 1998, **281**, 531-533.
117. B. A. Friesen, A. Bhattarai, U. Mazur and K. W. Hipps, *Journal of the American Chemical Society*, 2012, **134**, 14897-14904.
118. M. O. Blunt, J. Adisoejoso, K. Tahara, K. Katayama, M. Van der Auweraer, Y. Tobe and S. De Feyter, *Journal of the American Chemical Society*, 2013, **135**, 12068-12075.

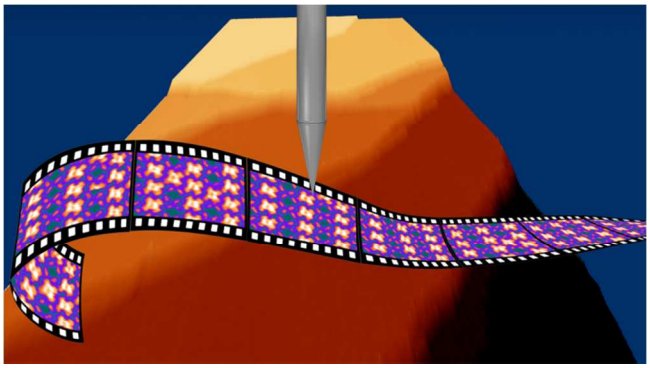

Scanning tunnelling microscopy of the dynamics of functional molecules (porphyrins) close to room temperature enables a detailed determination of the thermodynamic potentials including entropic contributions of the underlying processes.